A new multi-channel Mach probe measuring the radial ion flow velocity profile in the boundary plasma of the W7-X stellarator

J. Cai[1,2,3], Y. Liang[3], C. Killer[4], S. Liu[1,3], A. Hiller[3], A. Knieps[3], B. Schweer[3], D. Höschen[3], D. Nicolai[3], G. Offermanns[3], G. Satheeswaran[3], M. Henkel[3], K. Hollfeld[3], O. Grulke[4], P. Drews[3], T.Krings[3], Y. Li[1,3] and W7-X team

[1] *Institute of Plasma Physics, Chinese Academy of Sciences, PO Box 1126, Hefei 230031, People's Republic of China*

[2]*University of Science and Technology of China, Hefei 230026, People's Republic of China*

3 Forschungszentrum Jülich GmbH, Institut für Energie- und Klimaforschung–Plasmaphysik , Partner of the Trilateral Cluster (TEC), 52425 Jülich, Gremany

[4]*Max-Planck-Institut für Plasmaphysik Teilinstitut Greifswald, Wendelsteinstr. 1, 17491 Greifswald, Germany*

E-mail: j.cai@fz-juelich.de

Abstract

Ion flow velocity measurement in the edge and scraper-off layer (SOL) region is beneficial to understand the confinement related phenomenon in fusion devices such as impurity transport, and plays an important role in impurity control. During the Wendelstein 7-X (W7-X) operation phase 1.2a (OP1.2a), a multi-channel (MC) Mach probe mounted on the multi-purpose manipulator (MPM) has been used to measure radial profiles of edge ion flow velocity. This MC-Mach probe consists of two polar and two radial arrays of directional Langmuir pins (28 pins in total) serving for different aims, of which the polar arrays could obtain a polar distribution of ion saturation current while the radial arrays can be used to study the dynamic process of radially propagated event. In this paper, we report the observation of the radially outward propagation of a low frequency mode with a speed of around 200 m/s. The first measurement of radial

ion flow velocity profile using the MC-Mach probe in the boundary plasma of W7-X with island divertor will also be presented.

1. Introduction

Ion flow velocity measurement in the edge and scraper-off layer (SOL) region is of benefit to understand the confinement related phenomenon in fusion devices such as impurity transport,[1] and plays a crucial role in impurity control.[2] A lot of attempts have been made to measure the ion flow velocity, including Doppler shift measurement of impurity lines[3, 4] and probe measurement[5], in which the Mach probe[6] is the cheapest and simplest one. In general, the most common Mach probe is a parallel Mach probe aligned to magnetic field lines, consisting of two directional pins mounted on the opposite side of an insulator. The parallel Mach number (the ratio of parallel ion flow velocity to ion sound speed) can be deduced from the ratio of the upstream to the downstream ion saturation current collected by probe pins.[5] A more complex Mach probe is a Gundestrup Mach probe consisting of several directional pins mounted around an insulator at the different angle.[7] In addition to the parallel flow, the perpendicular (poloidal) flow caused by $\vec{E} \times \vec{B}$ drift will exist as well in the case of a strong radial electric field in the edge and SOL region. This setup allows to measure the perpendicular Mach number since the ion saturation current collected by inclined pins is sensitive to the perpendicular flow.

Wendelstein 7-X (W7-X), one of the world's largest and most advanced stellarators, has an intrinsic magnetic island chain at the boundary and aims for the demonstration of high performance steady-state plasma operation. The effect of magnetic islands on plasma flow has been demonstrated and the phenomenon that the perpendicular flow reverses at the center of the magnetic island has been observed on LHD[8] and TJ-II[9]. To study the effect of magnetic islands of W7-X on plasma flow, a multi-array Mach probe, which includes 8 rows in the radial direction and 28 pins in total, has been successfully commissioned and put into use on W7-X.

The rest of this paper is organized as follow: the related diagnostic setup will be

presented in section 2, followed by the presentation of the preliminary measurement of radial ion flow velocity profile in section 3. The discussion and conclusion will be given in section 4.

2. Diagnostic setup

W7-X is equipped with a multi-purpose manipulator (MPM) system[10], which acts as a carrier system for various probe heads. It is located near the outer midplane of module four at flange AEK40 (toroidal angle 200.7°), as Fig. 1 shows. The MPM system is able to insert the probe head into the plasma edge with a maximum stroke depth of 350 mm and a maximum acceleration of 30 m/s^2, both of which could be controlled and adjusted by a PLC system[11], making it possible to measure the radial profile within the SOL region as well as crossing the last closed flux surface (LCFS). For this campaign, the stroke position in terms of major radius is 6.06-6.08 m, which is limited by the hazard of arc striking. When the probe head is plunged too deep in a high performance discharge, the ion saturation current collected by the front pins will increase rapidly to more than 10 A, which can be harmful to electronic elements. Laser sensors has been used to monitor the position of the probe head during plunging with an uncertainty of 0.2 mm.

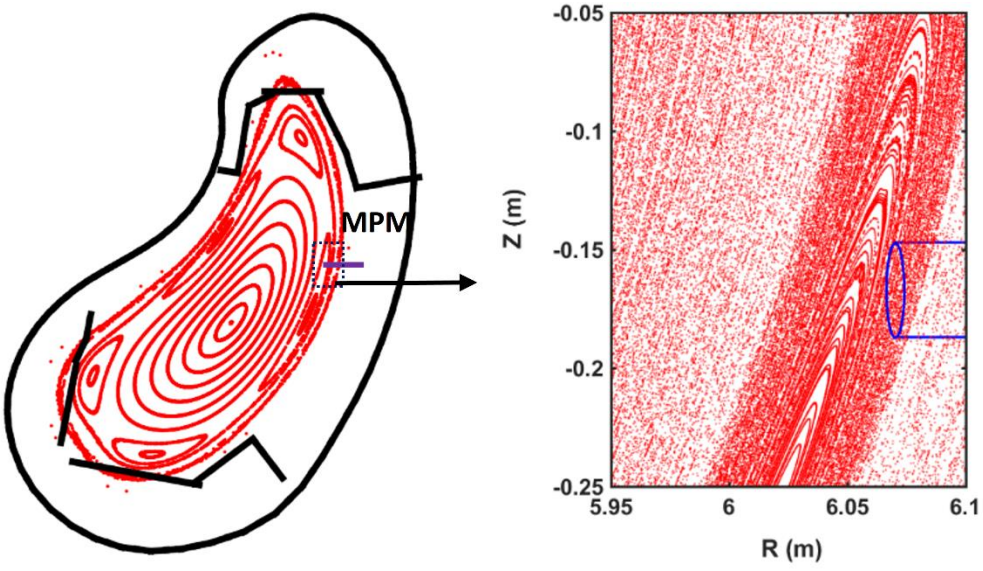

FIG. 1. The Poincare diagram at toroidal angle 200.7◦ in the standard configuration EJM on W7-X.

The position of the multi-purpose manipulator in the discharge #171206025 is labelled by the blue line, and the black lines represent divertor targets and outer vacuum vessel. The size of probe head relative to the size of magnetic island could been seen from the enlarged drawing of the island region.

As Fig. 2a shows, the probe head is constructed in the shape of a cylinder whose diameter of cross section is 42 mm and total length is 79 mm. There are 28 pins made of tungsten located around the cylindrical rod because of its high resistance to heat loads. As seen in Fig. 2b, these pins are flush mounted to the surface of the probe head cover instead of standing proud in the plasma, which enables the pins to collect the ion saturation current directionally. Each pin is isolated from its radially adjacent pins by an isolator between them, and the radial distance between adjacent pins is 6 mm. The area of each pin is approximately 11 mm^2, and the effective collecting areas of two pins in the opposite side are supposed to be identical. Thus, in the later calculation, the ratio of saturation current density could be replaced by the ratio of saturation current.

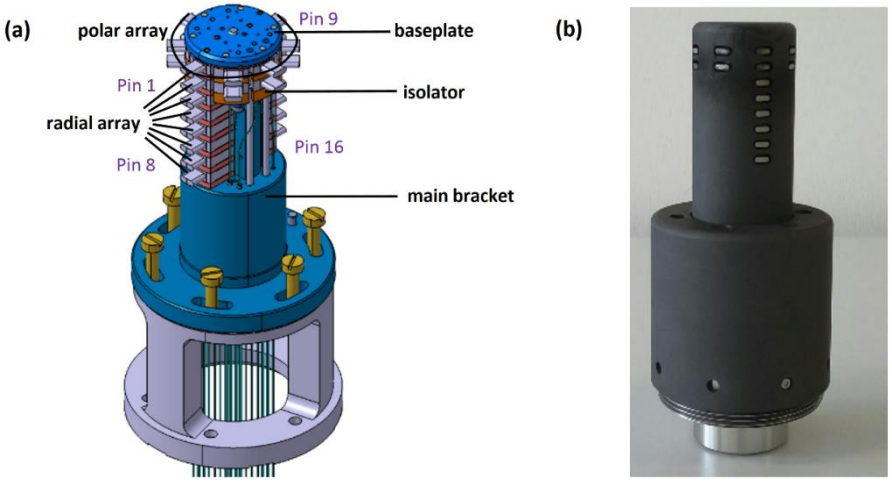

FIG. 2. Design of the Mach probe head without cover (a) and the picture of the Mach probe head (b). The orange parts are isolators and the silver parts are pins. Some pins have been labelled in the diagram by blue text. The pins of radial array seen in the diagram is labelled as 1-8 from top to bottom, and the pins on the opposite is labelled as 9-16. The pins in the first polar array is labelled as 1, 18, 20, 22, 9, 23, 26 and 27 counterclockwise while the pins in the second array is labelled as 2, 17, 19, 21, 10, 24, 25 and 28.

For a simple parallel Mach probe, there are only two directional pins located in the opposite side. In this Mach probe head, 8 pins are evenly located around the cylindrical rod in the first two rows, respectively, working as a Gundestrup Mach probe. This setup is able to obtain the polar distribution of ion saturation current, and consequently the perpendicular and parallel ion flow velocity can be deduced [7]. Another 12 pins are radially mounted in 6 rows back to back, measuring a radial profile of ion flow velocity simultaneously. The radial array, as one of the characteristics of this Mach probe head, could also be used to study the dynamic process of radially propagated events, such as bursts, modes caused by MHD instabilities and the perturbation of density and temperature caused by modulations.

A probe head cover made of graphite has been used to protect the interior part from the unwanted direct contact with plasma, as shown in Fig. 2b. Graphite has been chosen because of its high heat resistance, by which it could protect the interior part against the high heat loads from the hot plasma, especially those caused by electron cyclotron resonance heating (ECRH) stray radiation, and of its good mechanical stability under a high acceleration. However, in this campaign the graphite cover has been observed to be more likely to give rise to arc striking, which has limited the plunge depth of the probe head. For this reason, boron nitride has been chosen as the material of the Mach probe head instead of graphite for the next campaign OP1.2b.

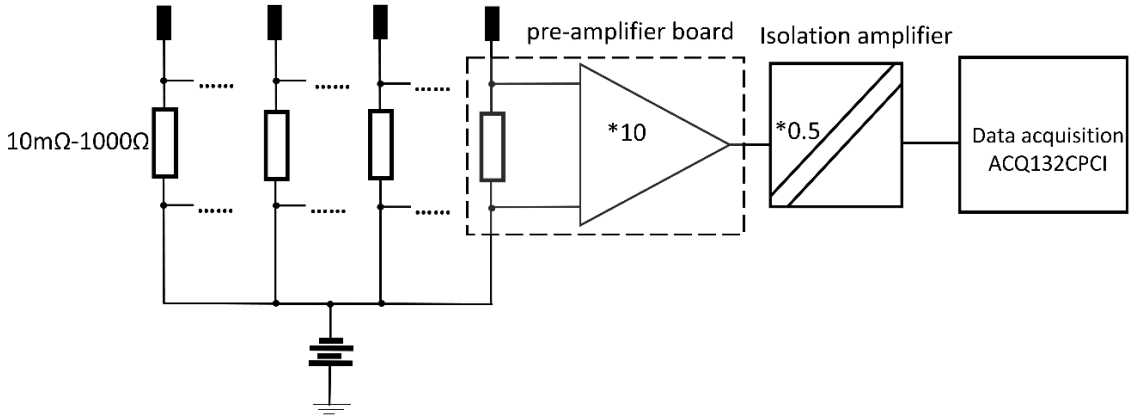

FIG. 3. The simplified circuit diagram of Mach probe. In this circuit diagram, the amplifiers and the data acquisition system of the first three pins are omitted.

To perform ion saturation current measurements, a biasing voltage of -160 V with

respect to the W7-X plasma vessel is applied to these pins, provided by integrated capacitor arrays in which one unit is used to bias four Mach pins, as shown in Fig. 3. The ion saturation current signal is converted into the voltage signal by a pre-amplifier with a gain factor from 0.1 V/A up to 1000 V/A, which could be adjusted depending on the magnitude of the saturation current. A 32-channels data acquisition system with 2 MHz sampling rate and 14 bit effective resolution has been used to convert the voltage signal to digital numeric values. An isolation amplifier has been used to isolate each channel of the probe system from the data acquisition system for the aim of avoiding grounding problems and to allow shunt measuring at high potential.

3. The model for Mach probe interpretation

The Mach number can be expressed as an exponential form of the ratio of the upstream ion saturation current density to the downstream ion saturation current density,

$$J_{\mathrm{up}}/J_{\mathrm{down}} = \exp\left(K\mathrm{M}_{//}\right), \tag{1}$$

which has been demonstrated theoretically and experimentally[5, 12-14]. In these fluid models of Mach probe, the formula has the same exponential form while the calibration factor K is varied depending on the various plasma parameters, such as ion temperature [5], viscosity [13, 14] and collisionality.

The magnetic field in the edge region on W7-X is 2.2-2.3T, and the ion larmor radius is around 0.19 mm [15], much smaller than the size of Mach probe pins 2 mm. As a consequence, the theory of magnetized plasma is suitable to interpret the experiment data on W7-X. What's more, in the experiment on W7-X, not only the parallel Mach number but also the perpendicular one is of interests to us. Therefore, a fluid model in magnetized plasma which takes account of the perpendicular drift has been used to deduce the parallel and also perpendicular Mach number.[16] The formula is given as

$$J_{\mathrm{up}}/J_{\mathrm{down}} = \exp[K(M_{//} - M_{\perp}cot\theta)] \tag{2}$$

, where θ is the angle between the magnetic field line and the collecting surface of pins, and the calibration factor K lies between 2.3 and 2.5. Similar formula has also been

given by another 2D fluid model using a self-similar method [17, 18], which indicates the same exponential form and the difference between the two formulas is the calibration factor K=2 in the latter 2D fluid model. In this paper, K is always taken as K=2.5 when deducing the Mach number.

Eq. (2) shows that the parallel Mach number could be deduced directly from the ratio of currents measured by the pins whose collecting surface is perpendicular to the field lines (θ=90°), while another ratio of currents measured by pins with a different orientation angle is required for the deduction of the perpendicular Mach number. In the previous experiments on CASTOR tokamak[19], it has been demonstrated that this model fits well with the measurements while θ lies between 30° and 150°, so the pin 19, 25, 20 and 26 (θ=0°) have been excluded for the data interpretation. In addition, the pin 18, 22 and 24 in the polar arrays have been open circuited during the assembling. As a consequence, the perpendicular Mach number can't be deduced by the pins in the first row because of the defective relevant pins used for deducing, while the perpendicular Mach number can be deduced from the difference between the ratio of currents measured by pin 2 to pin 10 and that measured by pin 21 to pin 28 in the second row.

$$M_{//} = \frac{lnR_1}{\mathrm{K}}, R_1 = J_2/J_{10}. \tag{3}$$

$$M_{\perp} = \frac{lnR_1}{\mathrm{K}} - \frac{lnR_2}{\mathrm{K}}, R_2 = J_{21}/J_{28}. \tag{4}$$

Since the field line is not strictly perpendicular to the collecting surface of the radial array on this experiment, the effect of misalignment on parallel and perpendicular flow should be taken into consideration. The effect of misalignment on flow velocity has been given analytically,[19]

$$M_{\perp}^{*} \approx M_{\perp}$$

$$M_{//}^{*} \approx M_{//} - M_{\perp}\,\Delta\,\theta, \tag{5}$$

where the Mach number with a star superscript is the actual value of Mach number, and $\Delta\,\theta$ is the angle misalignment. The misalignment has little effect on the perpendicular flow velocity while it could affect the parallel flow speed only if the product of perpendicular flow and the misalignment angle is big enough. In this campaign, the misalignment angle is not more than 8° (0.14 radians), consequently the effect of the

misalignment on the flow speed is negligible.

4. Preliminary experiment results

The Mach probe head has been successfully commissioned and used at the recent experiment of OP1.2a campaign on W7-X. Fig. 4 shows the basic parameters of discharge #171206025 at this campaign, whose magnetic configuration is EJM (standard configuration with five independent magnetic island in the edge) with the magnetic field direction being reversed compared to the default setup, indicating that the direction of toroidal magnetic is clockwise when viewing from the top.

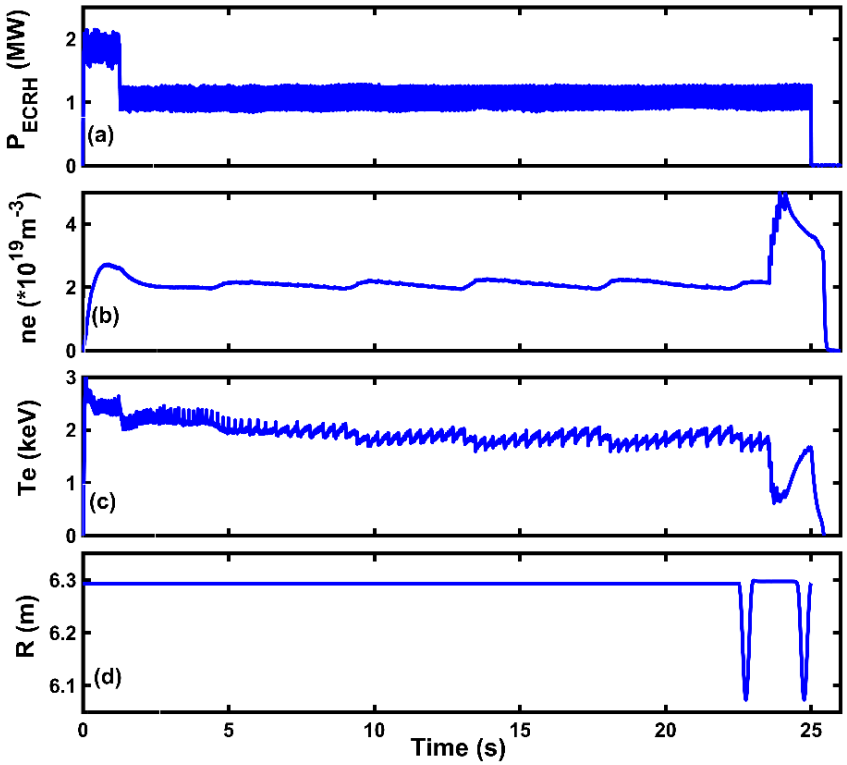

FIG. 4. Main parameters of shot #171206025. The diagram from the top to bottom is ECRH heating power, the core line-integrated density measured by interferometry, the core electron temperature measured by ECE and the position of the Mach probe head.

Pellet injection has been used at the end of the discharge, consequently there is a remarkable increase on the electron density and a decrease on the electron temperature.

The probe head has been plunged into the plasma edge twice, and the analysis of the data during the first plunge could be seen in Fig. 6. During the first plunge, the Electron Cyclotron Resonance Heating (ECRH) [20] heating power is 1 MW, line-integrated density measured by interferometry [21] is 2.15×10^{19} m^{-3} and the core electron temperature measured by Electron Cyclotron Emission (ECE) [22] diagnostic is 1.8 keV.

Fig. 5 shows the raw and filtered data of ion saturation current from pin 1 to pin 4 during the first plunge in discharge #171206025, of which a low pass filter with a cut-off frequency of 300 Hz has been used to smooth the raw saturation current signal. The ion saturation current of pin 4 is much lower than pin 1, indicating a quick decay of ion saturation current along the radial direction, which could be seen in Fig. 6a as well.

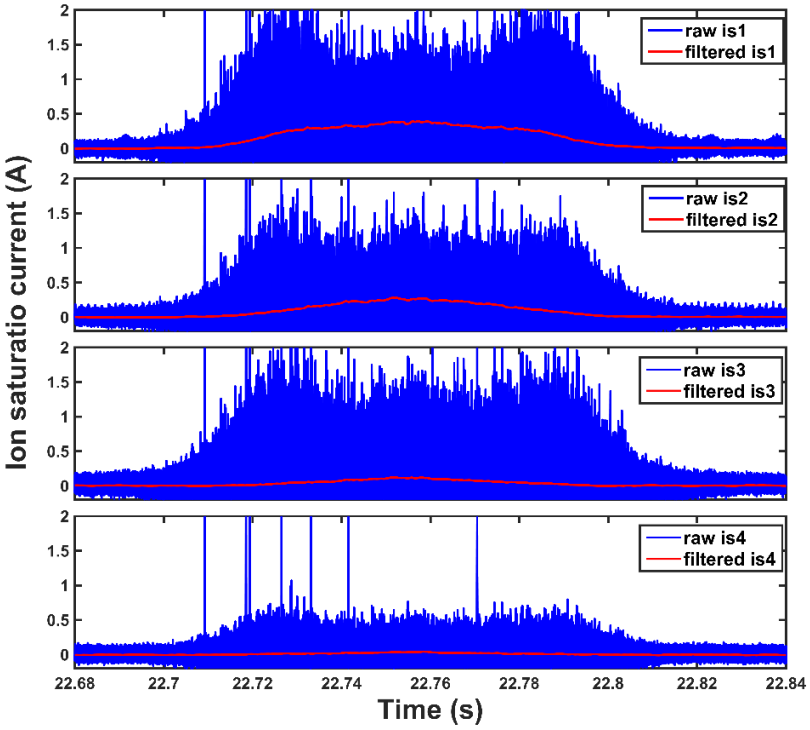

FIG. 5. The raw and filtered data of ion saturation current from pin 1 to pin 4 during first discharge in discharge #171206025.

Fig. 6 shows the measurement of radial profiles of ion saturation current and Mach number during the first plunge in discharge #171206025. As seen from Fig. 6a, the profiles of ion saturation current from pin 1 to pin 4 show a good repeatability. When the distance is greater than 6.09 m, the value of ion saturation current becomes

insignificant because of the low ion density and temperature there. Since the parallel Mach number is determined by the ratio of current density, the precision of Mach number would be strongly affected by deviations of measurement when the current signal is low, which could be seen in Fig. 6b. The radial profiles of the parallel Mach number deduced from the pins of first four rows show the same monotonically increasing trend and a good repeatability, as the profiles of ion saturation current do. Whereas when the distance is greater than 6.09 m, the profiles don't overlap very well. The perpendicular Mach number in the first row is missing because of the defective relevant pins used for deducing. The parallel flow direction is clockwise when viewing from the top, and the perpendicular flow direction is downward.

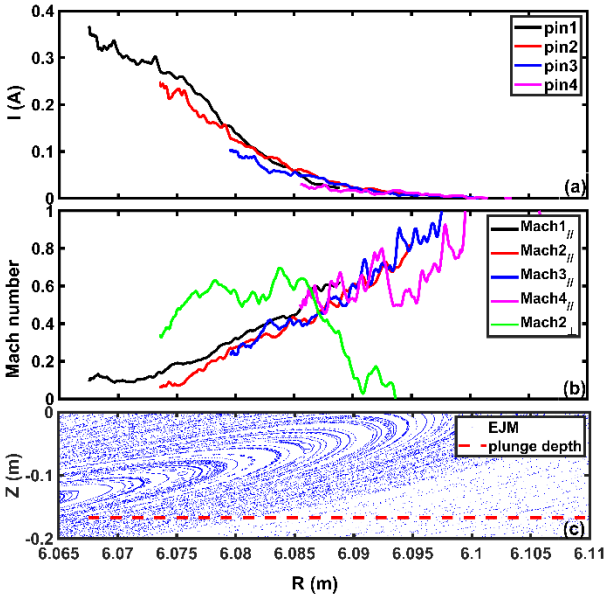

FIG. 6. The result of shot #171206025. The diagrams from the top to bottom are the radial profiles of ion saturation current from pin 1 to pin 4, the radial profiles of perpendicular and parallel Mach number and the Poincare picture of the island regime in EJM configuration.

Fig. 7a is the auto power spectrum of pin 9 in the discharge #171205027, and a low frequency mode below 5 kHz can be observed when the probe is inserted into the plasma deep enough (R > 6.10 m). To study the radial propagation of this low frequency mode, the relevant component of this signal has been extracted using a 1-5 kHz band-pass filter. Fig. 7b shows the cross-correlation of the 1-5 kHz band-pass filtered signal

of pin 9 with those measured by the entire radial array (pin 9 to pin 16), and a clear radially outward propagation with a velocity of around 200 m/s can be seen.

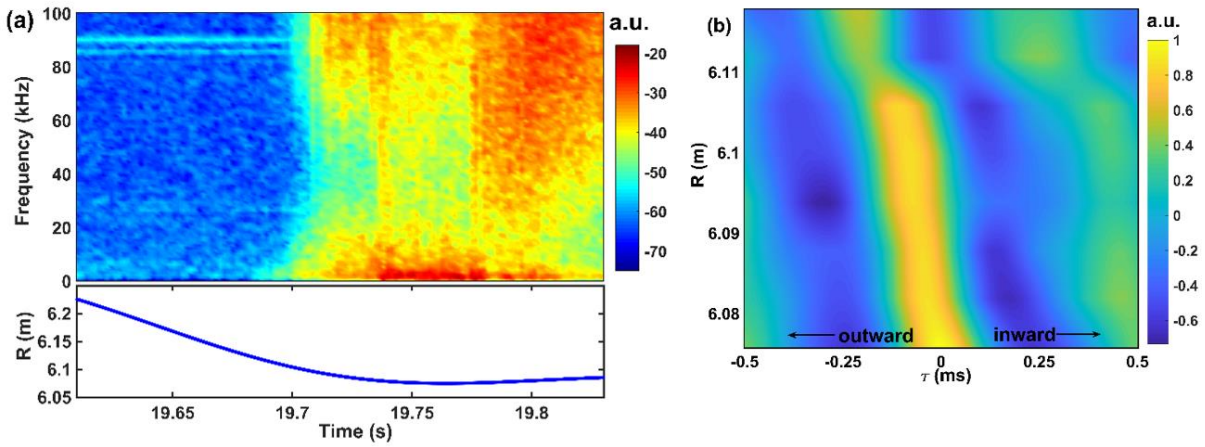

FIG. 7. (a) The auto power spectrum of pin 9 in the discharge #171205027 and (b) the cross-correlation between the 1-5 kHz band-pass filtered signal measured by pin 9 with those measured by other radial pins 9-16, which indicates the mode of 1-5 kHz propagates outwardly with a speed of around 200 m/s.

5. Discussion and conclusion

In addition to the radial propagation of the modes with different frequency, the dynamic process of the density perturbation caused by modulations is also one of the major research objects of the Mach probe head. Future experiments in the second divertor campaign on W7-X (OP1.2b) will include the analysis of the radial propagation of the density perturbation induced by gas puffs, which can be well studied using the radial array of Mach probe.

Although several pins of polar arrays are open circuited during the assembling, the results of the perpendicular and parallel Mach number are less affected. For future experiments in the second divertor campaign on W7-X (OP1.2b), a new inner-side design will be used to make the assembly process more robust. What's more, a new Mach probe head whose cover is made of insulated boron nitride instead of graphite

has been designed to reach deeper plunges which will then allow to assess plasma flow in the entire island. In addition, a gas feeding pipe has also been applied to the new Mach probe head to allow for gas puffing.

In conclusion, the multi-channel Mach probe head has been successfully commissioned and put into use on W7-X OP1.2a campaign, and the radial profile of parallel and perpendicular flow velocity have been obtained by the Mach probe head. The dynamic process of radially propagated mode has also been studied by the radial array of the Mach probe head, and a low frequency mode of 1-5 kHz propagating outward with a speed of around 200 m/s has been observed.

Acknowledgments

This work has been carried out within the framework of the EUROfusion Consortium and has received funding from the EURATOM research and training programme 2014–2018 under grant agreement no. 633053. The views and opinions expressed herein do not necessarily reflect those of the European Commission. The support provided by China Scholarship Council (CSC) is also acknowledged. Finally, the support by W7-X Team is acknowledged as well.

References

[1]R.C. Isler, Nucl. Fusion **23,** 1017 (1983).
[2]J. Neuhauser, W. Schneider and R. Wunderlich, Nucl. Fusion **24,** 39 (1984).
[3]M. G. Bell, Nucl. Fusion **19,** 33 (1979).
[4]S. Suckewer, H. P. Eubank, R. J. Goldston, E. Hinnov and N. R. Sauthoff, Physical review letters **43,** 207 (1979).
[5]M. Hudis and L. M. Lidsky, Journal of Applied Physics **41,** 5011 (1970).
[6]K.-S. Chung, Plasma Sources Science and Technology **21,** 063001 (2012).
[7]C. S. MacLatchy, C. Boucher, D. A. Poirier and J. Gunn, Review of Scientific Instruments **63,** 3923 (1992).
[8]K. Ida, N. Ohyabu, T. Morisaki, Y. Nagayama, S. Inagaki, K. Itoh, Y. Liang, K. Narihara, A. Y. Kostrioukov, B. J. Peterson, K. Tanaka, T. Tokuzawa, K. Kawahata, H. Suzuki and A. Komori, Physical review letters **88,** 015002 (2002).
[9]T. Estrada, E. Ascas ̃ar, E. Blanco, A. Cappa, C. Hidalgo, K. Ida, A. L ́opez-Fraguas and B. P. van Milligen, Nuclear Fusion **56,** 026011 (2016).
[10]D. Nicolai, V. Borsuk, P. Drews, O. Grulke, K. P. Hollfeld, T. Krings, Y. Liang, C.

Linsmeier, O. Neubauer, G. Satheeswaran, B. Schweer and G. Offermanns, Fusion Engineering and Design **123,** 960 (2017).
[11]G. Satheeswaran, K. P. Hollfeld, P. Drews, D. Nicolai, O. Neubauer, B. Schweer and O. Grulke, Fusion Engineering and Design **123,** 699 (2017).
[12]P. C. Stangeby, Physics of Fluids **27,** 2699 (1984).
[13]K. S. Chung, Physics of Plasmas **1,** 2864 (1994).
[14]I. H. Hutchinson, Physical Review A **37,** 4358 (1988).
[15]P. Drews, Y. Liang, S. Liu, A. Krämer-Flecken, O. Neubauer, J. Geiger, M. Rack, D. Nicolai, O. Grulke, C. Killer, N. Wang, A. Charl, B. Schweer, P. Denner, M. Henkel, Y. Gao, K. Hollfeld, G. Satheeswaran, N. Sandri and D. Höschen, Nuclear Fusion **57,** 126020 (2017).
[16]H. Van. Goubergen, R. R. Weynants, S. Jachmich, M. Van. Schoor, G. Van. Oost and E. Desoppere, Plasma Physics and Controlled Fusion **41,** L17 (1999).
[17]I. H. Hutchinson, Physical review letters **101,** 035004 (2008).
[18]I. H. Hutchinson, Physics of Plasmas **15,** 123503 (2008).
[19]J. P. Gunn, C. Boucher, P. Devynck, I. Ďuran, K. Dyabilin, J. Horaček, M. Hron, J. Stöckel, G. Van Oost, H. Van Goubergen and F. Žáček, Physics of Plasmas **8,** 1995 (2001).
[20]V. Erckmann, P. Brand, H. Braune, G. Dammertz, G. Gantenbein, W. Kasparek, H. P. Laqua, H. Maassberg, N. B. Marushchenko, G. Michel, M. Thumm, Y. Turkin, M. Weissgerber and A. Weller, Fusion Science and Technology **52,** 291 (2017).
[21]K. J. Brunner, T. Akiyama, M. Hirsch, J. Knauer, P. Kornejew, B. Kursinski, H. Laqua, J. Meineke, H. Trimiño Mora and R. C. Wolf, Journal of Instrumentation **13,** P09002 (2018).
[22]S. Schmuck, H. J. Hartfuss, M. Hirsch and T. Stange, Fusion Engineering and Design **84,** 1739 (2009).